nature methods

BRIEF COMMUNICATION

https://doi.org/10.1038/s41592-020-0819-7

Deep three-photon imaging of the brain in intact adult zebrafish

Dawnis M. Chow[1,3], David Sinefeld[2,3], Kristine E. Kolkman[1,3], Dimitre G. Ouzounov[2], Najva Akbari[2], Rose Tatarsky[1], Andrew Bass[1], Chris Xu[2]✉ and Joseph R. Fetcho[1]✉

Behaviors emerge from activity throughout the brain, but noninvasive optical access in adult vertebrate brains is limited. We show that three-photon (3P) imaging through the head of intact adult zebrafish allows structural and functional imaging at cellular resolution throughout the telencephalon and deep into the cerebellum and optic tectum. With 3P imaging, considerable portions of the brain become noninvasively accessible from embryo to sexually mature adult in a vertebrate model.

Vertebrate behavior emerges from interactions of neurons spread widely throughout the brain, but noninvasive monitoring of neuronal activity at single cell resolution is limited. Translucent larval zebrafish allowed for the first noninvasive calcium imaging in vertebrate neurons, setting the stage for the burgeoning use of zebrafish for functional studies[1–7]. In contrast, opaque adult zebrafish (Fig. 1a) are less tractable for deep noninvasive approaches, although important imaging has been done of more accessible regions, mostly in brain explants[8,9] and, in one case, initial structural 3P imaging in the telencephalon of intact adult zebrafish[10]. Here we evaluate noninvasive long-wavelength 3P imaging in adult zebrafish and image through the telencephalon and deep into the optic tectal and cerebellar regions, three widely studied brain regions.

We imaged brains in 3- to 7-month-old adults ($N=41$) in the Casper strain, which lacks pigments in the skin, to minimize pigment interference[11] (Fig. 1a,b). Using custom-built 3P imaging systems[12,13], we mainly performed structural and functional imaging at 1,300 nm, where green light-emitting calcium indicators are optimized, with additional structural imaging at 1,700 nm with red light-emitting fluorophores. We simultaneously collected the third harmonic generation (THG) signal to visualize surface structures, fiber tracts, blood vessels and blood flow (to assess viability)[14] (Extended Data Figs. 1 and 2 and Supplementary Video 1). We used small to medium-sized adults (mean standard length, tip of the head to base of the tail, 20.0 mm; range, 14.1–24.2 mm) to maximize optical access to the brain. Computerized tomography (CT) scan images showed that brain regions vary in depth and the thickness of the overlying skull (about 50–115 µm) and muscle (Fig. 1b,c), all of which may influence imaging success.

To assess in vivo optical properties of intact living zebrafish using 3P illumination, we imaged blood vessels labeled by retro-orbital injection of fluorescein or Texas red dextran to determine the decay of signal with depth (scattering length) at 1,300 or 1,700 nm in telencephalon, optic tectum and cerebellum (Fig. 1d and Supplementary Table 1). The telencephalon exhibited the longest scattering length (lowest decay with depth), consistent with its more translucent appearance as compared to optic tectum and cerebellum. We measured shorter scattering lengths in optic tectum and cerebellum and assessed signal-to-background ratio for labeled blood vessels and GCaMP6s-labeled nuclei at different depths in the three brain regions studied (Extended Data Fig 3). The upper bound for the axial resolution was ~2.9 µm (Extended Data Fig. 4) at ~200 µm depth.

To determine safe imaging parameters, we explored both nonlinear (at the focal point) and linear (away from the focal point, 'heat') damage. To assess nonlinear damage, we focused on one shallow depth in the telencephalon or optic tectum, gradually raising the power until tissue damage was apparent both during imaging and in subsequent examination of resulting three-dimensional volumes near the imaging plane. We imaged the telencephalon in three adults within 200–300 µm of the skull surface at 4 Hz with a laser repetition rate of 333 kHz, similar to the parameters described in the Ca^{++} imaging section for calcium imaging. Tissue damage within the field of view began at 11.3 mW (276 µm depth), 8.9 mW (180 µm depth) and 12 mW (267 µm depth) (Supplementary Video 2). The zebrafish retained blood flow (as seen in the THG channel) in regions outside the targeted area in all cases. In our structural and functional imaging experiments, we used much lower powers of 2–5 mW in superficial imaging and carefully increased power with imaging depth to compensate for laser light attenuation by the tissue.

We tested linear damage at 1,300 nm by first locating a shallow region in the optic tectum with obvious blood flow and then scanning the laser beam on a plane +800 µm below that region while exposing the brain to increasingly higher laser powers for 10 min. No change in surface blood flow was seen after exposure at 148 and 162 mW ($N=1$ each). The actual maximal powers (up to 92 mW) we used for deep imaging at 1,300 nm were well below this power, indicating that linear damage from heating by the unfocused light is unlikely to occur at power levels useful for imaging.

We noninvasively imaged genetically labeled neurons in all three brain regions, focusing primarily on nuclear localized GCaMP6s under the elavl3 promoter, which produces sparse, widespread labeling in adults that assists regional identification[4,6,8,15]. We also successfully imaged zebrafish with glutamatergic neurons labeled with DSRed (*Tg(vglut2a:loxP-DsRed-loxP-GFP)*[16]), tdTomato (*Tg(vglut2a:mtdtomato)*) and GFP (*Tg(vglut2a:EGFP)*[17]).

In the cerebellar region, we imaged THG signal at about 800 µm below the surface of the head and GCaMP6s at 700–750 µm below (Fig. 1e). Individual optical sections also revealed larger nuclei more superficially and deeper tightly packed smaller ones, consistent with the disposition and size differences of Purkinje and granule cells (Fig. 1e)[17].

[1]Department of Neurobiology and Behavior, Cornell University, Ithaca, NY, USA. [2]Department of Applied and Engineering Physics, Cornell University, Ithaca, NY, USA. [3]These authors contributed equally: Dawnis M. Chow, David Sinefeld, Kristine E. Kolkman. ✉e-mail: cx10@cornell.edu; jrf49@cornell.edu

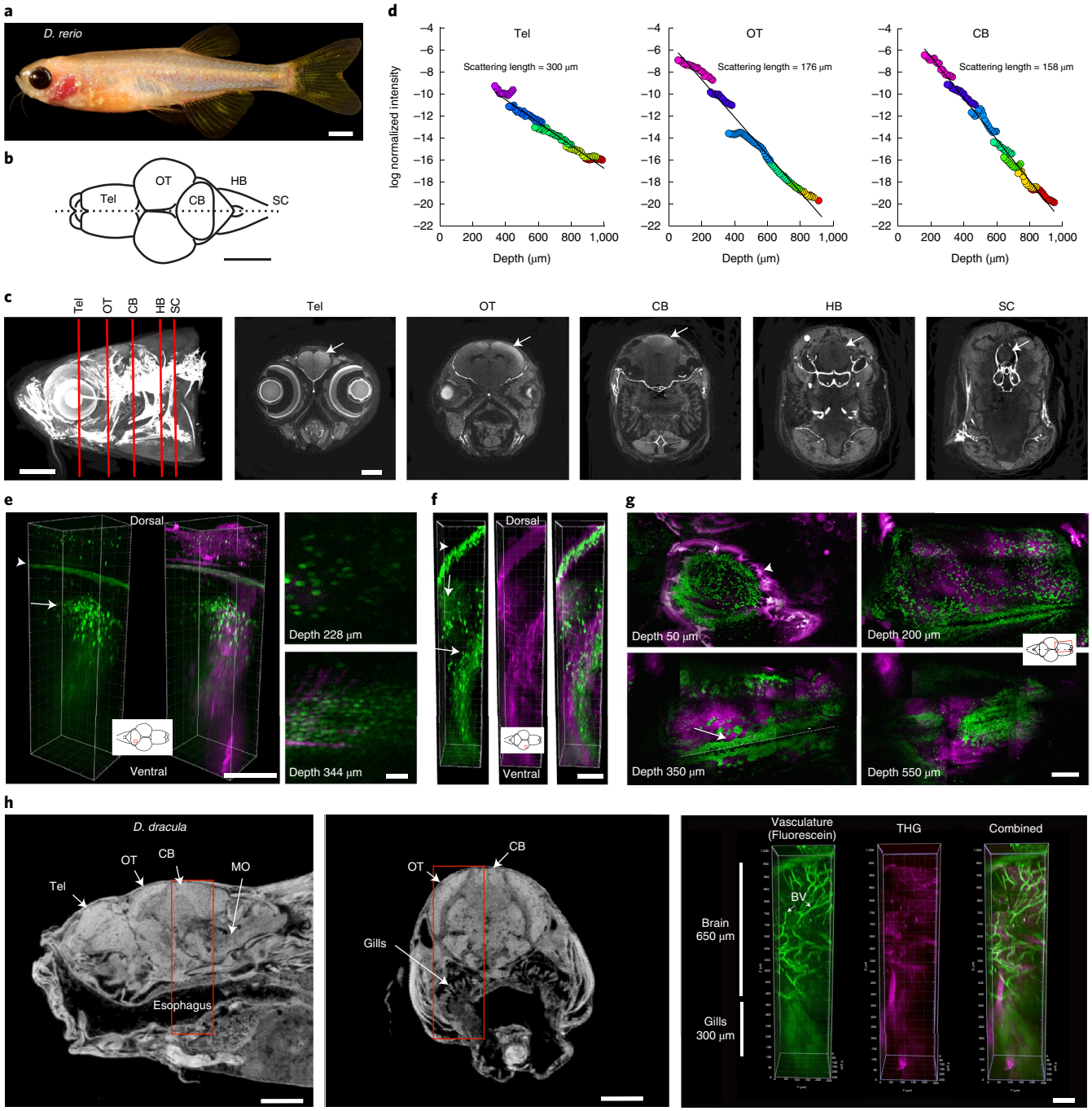

Fig. 1 | Imaging deep into zebrafish and *Danionella* brains. a, Adult zebrafish. Scale bar, 2 mm. **b**, Dorsal view of a zebrafish brain outline. Rostral is to the left. Tel, telencephalon; OT, optic tectum; CB, cerebellum; HB, hindbrain; SC, spinal cord. Scale bar, 1 mm. **c**, CT of a zebrafish head. Red lines are sections through the head in CT cross sections at the right. Arrows show the brain regions, labeled as in **b**. Scale bars, 1,000 µm (left) and 500 µm (Tel). White dot in in the hindbrain is muscle. **d**, Signal intensity versus depth from dye-labeled blood vessels to determine scattering lengths in labeled brain regions. Colors represent laser power, which increased with depth. **e**, Left side, three-dimensional view of 3P imaging into cerebellum of an intact zebrafish with nuclear localized GCaMP6s (*Tg(elavl3:H2B-GCaMP6s)*) (location of the imaged region shown in inset). GCaMP6s alone (green, on the left) and overlain with THG (magenta, on the right). Arrowhead, skull; arrow, neuronal nuclei. Right, single slices containing larger, presumptive Purkinje cell nuclei (top) and smaller likely granule cell nuclei (bottom). Scale bars from left to right; 200, 20, 20 and 100 µm. **f**, Three-dimensional reconstruction from optic tectum of a zebrafish with DSRed (shown in green) labeled glutamatergic neurons (*Tg(vglut2a:loxP-DsRed-loxP-GFP)*). Arrowhead, skull surface. Left panel arrows, processes of glutamatergic neurons (upper arrow) and a deeper cell layer. Middle panel, THG channel (magenta). Right, overlay of THG fibers and DSRed neurons. **g**, Optical sections from a montage of *Z* stacks through one entire half of the telencephalon of an intact zebrafish. Neuronal nuclei, green (*Tg(elavl3:H2B-GCaMP6s)*); THG, magenta. Rostral is to right. Arrowhead top left, skull. Dotted line, lower left is the midline of the telencephalon, with an arrow marking neurons along the midline. Scale bar, 100 µm. **h**, Left and middle panels, NanoCT scan of an adult *Danionella dracula* head. Arrows point to the main brain regions. Scale bars, 250 µm. Left panel, sagittal view, with rostral to the left. Middle panel, cross section through the region imaged with 3P (red box) before the CT. Right, 3P imaging of blood vessels filled with fluorescein imaged at 1,300 nm (green) and THG signal in magenta. BV, blood vessel. Scale bar, 100 µm. CT scan of zebrafish: $N=2$ fish. Decay length, $N=5$. Structural imaging; CB $N=10$, OT $N=16$ and Tel $N=12$. Danionella imaging, $N=2$ for CT and structure.

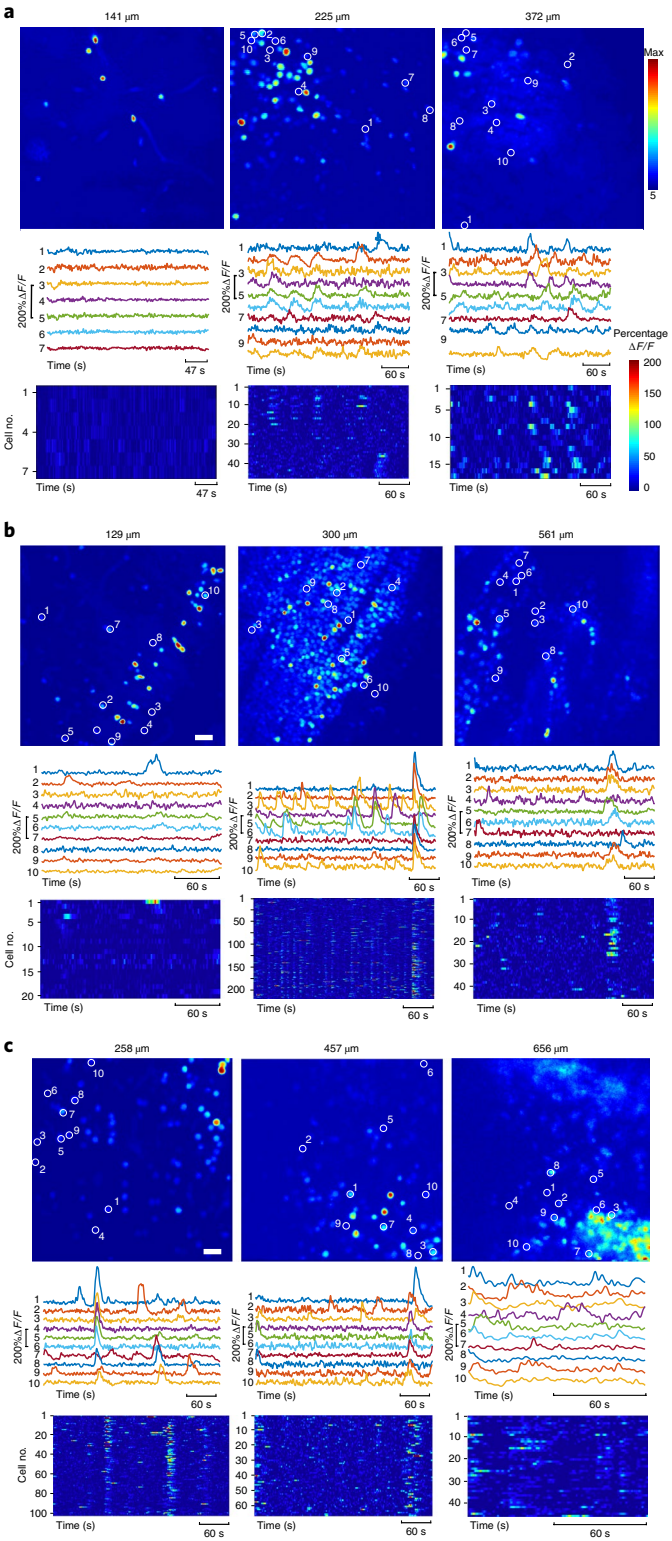

Fig. 2 | Functional imaging of main brain regions in intact adult zebrafish. **a**–**c**, Functional imaging in the *Tg(elavl3:H2B-GCaMP6s)* zebrafish at different depths in cerebellum (**a**), optic tectum (**b**) and telencephalon (**c**). In each panel, the top row shows, from left to right, optical sections at increasing depths in the indicated brain region. The images show raw fluorescence signal, averaged over the length of imaging with intensity mapped to the color bar at the right (red is the brightest pixel in each image and blue the dimmest). Middle row, Δ*F*/*F* traces from the numbered neurons in each frame. Bottom row, raster plots of Δ*F*/*F* intensity from neurons in the section. Lower right color bar maps the magnitude of the Δ*F*/*F* signal. Note that the duration of imaging in the deepest telencephalic regions was shorter than the others, so the time base is expanded. Cerebellum functional imaging; $N=2$ fish, OT $N=6$ and Tel $N=9$.

Imaging of glutamatergic neurons in the optic tectum revealed the known layering of fibers and cell bodies there[18], evident at both 1,700 nm (Fig. 1f, *Tg(vglut2a:loxP-DsRed-loxP-GFP)*[16]) and 1,300 nm (*Tg(vglut2a:EGFP)*[17]), not shown). In superficial layers of the optic tectum where cell bodies are sparse and axons and dendrites predominate, fiber layers were visible on the THG channel (Extended Data Figs. 1 and 2) as were fluorescently labeled cell bodies. In the deepest tectal imaging (roughly 750 µm below the surface of the head), we were able to reach the largest tectal cellular layer, the stratum periventriculare, which contains densely packed neurons[18].

The telencephalon, where 3P imaging of structural features has been previously achieved[10], was the most favorable region for imaging, consistent with its longer scattering length. We show imaging through the depth of the telencephalon (to 1,045 µm below the surface of the head) based on a montage of one complete side of the forebrain from a series of *Z* stacks containing neurons labeled with elavl3:GCaMP6s (Fig. 1g and Supplementary Videos 3 and 4). The 3P approach thus allows for noninvasive access to the entire forebrain of an intact adult vertebrate model system[19].

We also used blood vessel labeling to assess the achievable depth of 3P imaging in adult *D. dracula* ($N=3$), a member of a closely related genus containing emergent translucent fish models with smaller sized adults than zebrafish[20]. We imaged through the head, the deepest parts of the brain and beyond, as shown in paired CT and 3P images of the same fish (Fig. 1h).

Deep, noninvasive functional studies have proved challenging in adult zebrafish, in contrast to the extensive imaging possible in larval zebrafish[1,3,4,6]. We set out to overcome this barrier by performing functional imaging at different depths in the cerebellum, optic tectum and telencephalon (Fig. 2). We imaged spontaneous calcium transients deep into these regions and obtained good signal-to-noise ratio (Fig. 2 and Extended Data Figures 5 and 6). We were able to monitor calcium signals in over two hundred neurons in a 200 by 200 µm field of view in a densely labeled region of optic tectum (Supplementary Video 5). The deepest imaging was in the telencephalon where we could detect calcium transients at 750 µm into the head, near the ventral extent of this region. There was still a considerable calcium signal (over twofold increases) even in the deepest regions.

In sum, we show deep 3P noninvasive imaging in several principal, widely studied brain regions of mature adult zebrafish, including access to the entire forebrain of a vertebrate model. Large portions of a vertebrate brain are now accessible for noninvasive structural and functional studies from embryo to adult.

Online content

Any methods, additional references, Nature Research reporting summaries, source data, extended data, supplementary information, acknowledgements, peer review information; details of author contributions and competing interests; and statements of data and code availability are available at https://doi.org/10.1038/s41592-020-0819-7.

Received: 25 June 2019; Accepted: 24 March 2020;
Published online: 27 April 2020

References

1. Fetcho, J. R. & O'Malley, D. M. Visualization of active neural circuitry in the spinal-cord of intact zebrafish. *J. Neurophysiol.* **73**, 399–406 (1995).

2. Cox, K. J. & Fetcho, J. R. Labeling blastomeres with a calcium indicator: a non-invasive method of visualizing neuronal activity in zebrafish. *J. Neurosci. Methods* **68**, 185–191 (1996).
3. O'Malley, D. M., Kao, Y.-H. & Fetcho, J. R. Imaging the functional organization of zebrafish hindbrain segments during escape behaviors. *Neuron* **17**, 1145–1155 (1996).
4. Higashijima, S., Masino, M. A., Mandel, G. & Fetcho, J. R. Imaging neuronal activity during zebrafish behavior with a genetically encoded calcium indicator. *J. Neurophysiol.* **90**, 3986–3997 (2003).
5. Ahrens, M. B. et al. Brain-wide neuronal dynamics during motor adaptation in zebrafish. *Nature* **485**, 471–477 (2012).
6. Vladimirov, N. et al. Light-sheet functional imaging in fictively behaving zebrafish. *Nat. Methods* **11**, 883–884 (2014).
7. Andalman, A. S. et al. Neuronal dynamics regulating brain and behavioral state transitions. *Cell* **177**, 970–985 (2019).
8. Li, J. et al. Early development of functional spatial maps in the zebrafish olfactory bulb. *J. Neurosci.* **25**, 5784–5795 (2005).
9. Jacobson, G. A., Rupprecht, P. & Friedrich, R. W. Experience-dependent plasticity of odor representations in the telencephalon of zebrafish. *Curr. Biol.* **28**, 1–14 e13 (2018).
10. Guesmi, K. et al. Dual-color deep-tissue three-photon microscopy with a multiband infrared laser. *Light Sci. Appl.* **7**, 12 (2018).
11. White, R. M. et al. Transparent adult zebrafish as a tool for in vivo transplantation analysis. *Cell Stem Cell* **2**, 183–189 (2008).
12. Ouzounov, D. G. et al. In vivo three-photon imaging of activity of GCaMP6-labeled neurons deep in intact mouse brain. *Nat. Methods* **14**, 388–390 (2017).
13. Wang, T. et al. Three-photon imaging of mouse brain structure and function through the intact skull. *Nat. Methods* **15**, 789–792 (2018).
14. Farrar, M. J., Wise, F. W., Fetcho, J. R. & Schaffer, C. B. In vivo imaging of myelin in the vertebrate central nervous system using third harmonic generation microscopy. *Biophys. J.* **100**, 1362–1371 (2011).
15. Park, H. C. et al. Analysis of upstream elements in the HuC promoter leads to the establishment of transgenic zebrafish with fluorescent neurons. *Dev. Biol.* **227**, 279–293 (2000).
16. Satou, C., Kimura, Y. & Higashijima, S. Generation of multiple classes of V0 neurons in zebrafish spinal cord: progenitor heterogeneity and temporal control of neuronal diversity. *J. Neurosci.* **32**, 1771–1783 (2012).
17. Bae, Y.-K. et al. Anatomy of zebrafish cerebellum and screen for mutations affecting its development. *Dev. Biol.* **330**, 406–426 (2009).
18. Corbo, C. P., Othman, N. A., Gutkin, M. C., Alonso Adel, C. & Fulop, Z. L. Use of different morphological techniques to analyze the cellular composition of the adult zebrafish optic tectum. *Microsc. Res. Tech.* **75**, 325–333 (2012).
19. Diotel, N. et al. Comprehensive expression map of transcription regulators in the adult zebrafish telencephalon reveals distinct neurogenic niches. *J. Comp. Neurol.* **523**, 1202–1221 (2015).
20. Britz, R., Conway, K. W. & Ruber, L. Spectacular morphological novelty in a miniature cyprinid fish, *Danionella dracula* n. sp. *Proc. Biol. Sci.* **276**, 2179–2186 (2009).

Methods

Animal preparation. Adult zebrafish between 3 and 7 months postfertilization (Casper, *Tg(elavl3::H2B-GCaMP6s)*[6]; *Tg(vglut2a:loxP-DsRed-loxP-GFP)*[16]; *Tg(vglut2a:EGFP)*[17]; *Tg(vglut2a: mtdtomato)* were used. Zebrafish have indeterminate growth with the rate varying with parameters such as feeding and fish density, so adults can vary widely in size. We primarily chose small to medium-sized adults to facilitate the percentage of brain structure accessible with deep imaging (mean size in our experiments was 20 mm standard length (tip of head to base of tail), 14.1–24.2 mm range). Animals were anesthetized in 0.2 mg ml^{-1} tricaine solution (pH 7.2) and then injected with 2 µl of pancuronium bromide (0.4 µg µl^{-1} in Hanks). The zebrafish were stabilized by placing them in a 'V'-shaped groove cut in agar, and held in place by a Kimwipe draped over the zebrafish caudal to the head and glued onto the agar surface. A drop of bupivacaine was place on the surface of the head for anesthetic. Zebrafish were perfused through the mouth and over the gills at a rate of 2 ml min^{-1} with an ESI MP2 Peristaltic Pump (Elemental Scientific) with well-oxygenated temperature-controlled fish system water (4-l reservoir heated with a Finnex 800 W heater controlled via a Heater Controller set to 26.7 °C).

Adult *D. dracula* were anesthetized in 0.03% benzocaine solution and their vasculature labeled via injection of a 10% solution of dextran fluorescein (10,000 molecular weight, Invitrogen) into blood vessels in a highly vascularized region caudal to the operculum and rostral to the heart. Fish were stabilized by positioning them on a cured Sylgard 184 Silicone Elastomer-containing dish (Dow Consumer Solutions) and kept upright with stainless steel supports embedded in the cured Sylgard. Fish were perfused through the mouth and over the gills at a rate of 1 ml min^{-1} with an ESI MP2 Peristaltic Pump (Elemental Scientific) with well-oxygenated temperature-controlled fish system water (4-l reservoir heated with a Top Fin Betta Aquarium Heater set to 25 °C).

All procedures were in accord with the US National Institutes of Health guidelines for animal use in experiments, and were approved by Cornell University's Institutional Animal Care and Use Committee.

CT scanning of zebrafish and *Danionella*. Adult zebrafish were euthanized in tricaine solution. Whole zebrafish were fixed in 4% paraformaldehye at 4 °C for 48 h. They were then transferred to a solution containing 0.1% iodine metal and 0.2% potassium iodide in water until imaging 4 d later.

Zebrafish were scanned on a Zeiss Versa 520 CT scanner at 80 kV per 7 W. The instrument was set to yield a 4.9 µm resolution using a ×4 objective. The CT image was reconstructed from 2001 X-ray fluoroscopy images with an exposure time of 3 s each, using OptiReco v.12 and v.14. Skull thickness above telencephalon, optic tectum and cerebellum was measured on the CT by averaging three dorsal locations above each brain region.

Adult *Danionella* were euthanized in benzocaine solution. Whole fish were fixed in 4% paraformaldehyde at 4 °C for 24 h and then stained with 1% iodine metal and 2% potassium iodide. The stained fish was scanned at 120 kV per 10 W on the Zeiss Versa 520, using the ×4 objective and a resolution of 2.7 µm. The machine took 2,401 exposures of 0.7 s each, and the CT data was reconstructed using the standard Zeiss reconstruction software.

3P system. The 3P imaging was done with a previously published custom-built system[12,13]. A schematic description of the system is shown in Extended Data Fig. 7.

Experimental setup at 1,300 nm. *Excitation source.* The excitation source for 3PM at 1,300 nm was a noncollinear optical parametric amplifier (Spectra Physics) pumped by a regenerative amplifier (Spirit, Spectra Physics). The noncollinear optical parametric amplifier provided an average power of ~500 mW (1,250 nJ per pulse at 400 kHz repetition rate). A half-wave plate (HWP) and a polarization beamsplitter cube were used for power control.

Pulse compression. A two-prism (SF11 glass) compressor was used to compensate for the normal dispersion of the optics of the light source and the microscope, including the objective. The pulse duration (measured by second-order interferometric autocorrelation) under the objective was ~60 fs after optimizing the prism compressor (Extended Data Fig. 7).

Imaging setup. Images were taken with a custom-built microscope with a high-numerical aperture objective (Olympus XLPLN25XWMP2, 25×, numerical aperture of 1.05). The signal was epi-collected through the objective and then reflected by a dichroic beam splitter (FF705-Di01–25x36, Semrock) to the detectors. The detection system had two channels: one for the green fluorescence signal emitted by the calcium indicator and the other for the THG signal at λ = 433 nm. A 488-nm dichroic beam splitter (Di02-R488–25x36, Semrock) was inserted in the signal path at 45° between the two photomultiplier tubes (PMTs) to separate the THG and fluorescence. We used a PMT with GaAsP photocathode (H7422–40) for the fluorescence signal and an ultra bialkali PMT (R7600U–200) for the THG signal. The optical filters for the fluorescence and the THG channels were 520/60 and 420/40 bandpass filters (Semrock), respectively.

Experimental setup at 1,700 nm. *Excitation source.* The excitation source for 3PM at 1,700 nm was an optical parametric amplifier (Opera-F, Coherent) pumped by an amplifier (Monaco, Coherent). The excitation wavelength was ~1,680 nm. The average power of the source was ~330 mW (1,000 nJ per pulse at a 333-kHz repetition rate). A HWP and a polarization beamsplitter cube were used for power control.

Pulse compression. A 4-mm thick silicon plate was placed in the optical beam path to compensate for the anomalous dispersion of the optical elements of the light source and the microscope, including the objective. To maximize transmission, the silicon plate was placed at the Brewster's angle. The pulse duration (measured by second-order interferometric autocorrelation) under the objective was ~70 fs.

Imaging setup. Images were taken with a custom-built microscope with a high-numerical aperture objective (Olympus XLPLN25XWMP2, ×25, numerical aperture of 1.05). The signal was epi-collected through the objective and then reflected by a dichroic beam splitter (FF705-Di01-25x36, Semrock) to the detectors. The detection system had two channels: one for the red fluorescence signal emitted by DSRed or tdTomato and the other for the THG signal at λ = 560 nm. A 573-nm dichroic beam splitter (Di02-R561-25x36, Semrock) was inserted in the signal path at 45° between the two PMTs to separate the THG and fluorescence. We used a PMT with GaAsP photocathode (H7422–40) for the fluorescence signal and an ultra bialkali PMT (R7600U–200) for the THG signal. The optical filters for the fluorescence and THG channels were 593/40 and 556/25 bandpass filters (Semrock), respectively.

For both systems, the fish was placed on a motorized stage (M-285, Sutter Instrument Company). A computer running the ScanImage 3.8 module on MATLAB (MathWorks) software was used to control the stage translation and image acquisition. The PMT current was converted to voltage and amplified using a transimpedance amplifier (c7319, Hamamatsu). Analog-to-digital conversion was performed by a data acquisition card (NI PCI-6115, National Instruments).

The field of view ranged from 200 to 650 µm. The pixel rate for 3P imaging is limited by the repetition rate of the excitation source, which is lower than that in 2P imaging. The fast 4.25 Hz per frame scanning rate used for functional imaging corresponds to about one laser pulse per pixel. For activity imaging, however, signal from the entire nucleus was integrated to generate the activity trace. Depending on the exact size, a single neuron consists of tens to hundreds of pixels within the field of view. Therefore, the number of excitation pulses per neuron per frame is large, even at the limit of one excitation pulse per pixel, enabling a high frame rate at a relatively low repetition rate. For structural imaging, longer pixel dwell time and/or averaging over multiple frames eliminates any impact of the low repetition rate. More details of dwell times, averaging and so on for structural and functional imaging are given in subsequent sections.

Navigation around the head and brain of the fish. Navigation under the 3P imaging conditions initially proved challenging, as surface features under magnification, and using the THG channel, were not intuitive without familiarity. To ease navigation to known areas for imaging, we implemented a wider field of view light objective and white light imaging using a camera system to establish a relative coordinate system, defining reference points based on skull sutures and other anatomical features of the head. With experience, we were eventually able to more easily identify regions in single slices based on the THG signal from the surface structures, fiber patterns and the disposition of neurons (see Extended Data Figs. 1 and 2).

Decay length measurements. Decay lengths were quantified by examining signal intensities at different depths by imaging fluorescent dye injected into the bloodstream of wild-type unlabeled Casper zebrafish. Approximately 1 µl of the dye, (20% concentration, 500 kDa molecular weight fluorescein dextran or 70 kDa molecular weight Texas Red dextran in Hanks solution for 1,300 and 1,700 nm excitation, respectively) was injected by hand retro-orbitally on the morning of the experiment. Positively labeled zebrafish were screened by imaging the tail with a fluorescent dissecting microscope (Leica M205 FA) immediately after injection to look for clearly labeled blood vessels. For each region to be measured, stacks were taken at 5–10-µm steps starting deepest and moving shallower, and power was adjusted to avoid saturation of the PMTs and potential damage to the zebrafish.

For analysis, after background subtraction and averaging, regions containing blood vessels were segmented from the image for each slice using a custom MATLAB script to extract pixels 2–3 standard deviations above the mean intensity. An average signal intensity was produced for each slice by averaging the segmented pixels. Linear decay curves were fit to log(average signal / power^3) and reported as (3/slope) of the fit, which gives the length in micrometers through which the signal intensity will decay by a factor of 1×10^3. Alternatively, the top 0.1% of pixels was also identified as over 3.29 standard deviations above the background. The results were similar with both approaches.

Nonlinear and linear damage thresholds. Nonlinear damage was assessed in the telencephalon or optic tectum by imaging at 4.25 Hz (the rate used for our functional data) or 8.5 Hz for 4 min at a depth between 200 and 300 µm (including skin and skull) in the telencephalic or optic tectal regions with a repetition rate of 333 kHz in animals expressing GCaMP6s (*Tg(elavl3:H2B-GCaMP6s)*). When power was sufficiently high to start damaging tissue, damage was apparent during live imaging by sustained increase in brightness of GCaMP6s signals of

neurons followed by a development of absence in the signal that appears as a black area with a whiter halo, where the tissue damage was likely most severe (Supplementary Video 2).

Linear damage was assessed by examining the presence or absence of blood flow on the THG channel in living animals near the surface of the optic tectum after sustained exposure for 10 min to a beam of systematically varying power focused at a depth of 800 µm below the surface. Animals were considered heat-damaged if blood flow occurred pre-exposure in a region but not postexposure to deep imaging at the tested intensity. The overall viability of the animal was evident by assessing blood flow outside the exposed area.

Structural imaging. For structural imaging using both 1,300 and 1,700 nm excitation, the maximum power was limited to about 90 mW at the deepest depths imaged to ensure a lack of damage to the tissue. As this appeared to be well below the damage limit, it is possible that additional power usage could result in good signal-to-noise ratios at even greater depths than reported here. Surface imaging required approximately 3 mW power. As we imaged deeper into the brain, power and the number of averages per slice were increased. Structural images were collected at exposures of 6 µs per pixel and frame rates of 0.53 Hz, averaging 3–10 images depending on depth. The longest structural imaging, for the entire telencephalon lobe, took over 4 h, about three of which were actual scanning to collect the stacks.

For structural reconstructions, image stacks were assembled using a custom MATLAB (v.8,9) program autoAssembleStacks.m and Imaris (Bitplane). The program averaged .tif files and placed them according to the *z* coordinates present in the header of the ScanImage.tif files. To obtain a concatenated stack from substacks collected at increasing power with depth, each substack was normalized such that the 99th percentile of pixels was at 2^{15} (half the range of a 16-bit number). Overlaps between stacks were averaged.

For more complex multi-column assemblies, such as that of the entire telencephalon on one side of the brain, each averaged substack was normalized to a single shallow slice with many labeled cells. The intensities in the reference slice were converted into the range of (0, 2^{15}) and then the imhist function in MATLAB was used to compute a histogram. Histogram equalization of the other substacks was accomplished by using the histeq contrast matching function. The larger assembly was then produced by using image coordinates from the microscope motor and the program XUVstitch. Finally, the normalize layers function in Imaris was used, followed by median smoothing ($3 \times 3 \times 1$) to produce the final images.

Adult female *D. dracula* (three fish in total) with a range in standard length from 15.7–16.7 mm were imaged. We used an injection of fluorescein caudal to the operculum to fill blood vessels in the fish, which we then imaged intact and alive. One to three image stacks ranging in *z* depth from 400 to 1,000 µm were taken per fish at the midline near caudal midbrain and rostral cerebellum, where the brain is thickest in *z*. For structural imaging using 1,300 nm excitation, maximum imaging power was 13.6 mW at the deepest depths imaged. Surface imaging required at most 3 mW power after the objective. As we imaged deeper into the brain, power was increased. Structural images were collected at exposures of 6 and 13 µs per pixel and frame rates of 0.47 and 0.23 Hz, averaging 3–10 images, depending on depth. Figure 1h (right panel) shows an example imaging at 6 µs per pixel with a frame rate of 0.47 Hz. Images were assembled and viewed as for zebrafish above. While our imaging was 3P, *D. dracula* are so transparent that even 2P imaging may make much of their brain accessible.

Ca^{++} imaging. Ca^{++} imaging was performed in healthy animals as assessed by blood flow visible on the THG channel. Images were acquired at a 3-µs exposure per pixel and a frame rate of 4.25 Hz, at minimal power needed to visualize the label. As expected with the differences in decay length, the ability to functionally image deep into the zebrafish adult brain varied across the main brain regions. The changes in neuronal calcium could be observed in telencephalon at a depth greater than 600 µm (see Fig. 2, 656 µm). The deepest functional imaging in the optic tectum was at 561 µm, and the deepest calcium imaging in the cerebellum was at 372 µm. The powers used were well below those that led to linear or nonlinear damage in our testing of damage thresholds. Although most functional imaging sessions were about 4–5-min long at a given plane, we performed several longer experiments, including one calcium imaging experiment where we imaged continuously for 1 h at 4.25 Hz.

After acquisition of calcium imaging data, a correction was made for small lateral movements of the imaged region and background was subtracted. Cell segmentation was accomplished using Imaris (Bitplane). For each time point, a neuron's intensity was calculated as the mean of its segmented pixels. Traces were further processed by averaging subsequent frames (halving the frequency to 2.125 Hz), smoothed using a moving average of five frames and passed through a low-pass Butterworth filter with cutoff at 0.43 Hz. $\Delta F/F$ was calculated by using the median of a 60 s window around each point as the baseline.

For photon counts, instrument background was estimated from calcium imaging videos using the presence of shuttered pixels on the first frame of each video (approximately the first two lines). Subsequently, the mean-background-subtracted image intensity per neuron was multiplied by the number of pixels segmented for that neuron and divided by a constant factor 880 that was determined experimentally[12,13] as the scaling factor for photon counts of the instrumentation. Finally, flux was computed as a rate (photon counts per second per neuron) by multiplying the counts by the image acquisition frequency (typically 4.25 Hz).

Reporting Summary. Further information on research design is available in the Nature Research Reporting Summary linked to this article.

Data availability

The imaging and scattering length data sets that support the findings of this study are available from the corresponding author upon reasonable request.

Code availability

The software codes used for the analyses are available from the corresponding author upon reasonable request.

Acknowledgements

The work was supported by grant nos. NSF DBI-1707312, NIH 1U01NS103516, NSF IOS-1457108 and NIH S10OD012287. We thank C. Walcott (Cornell University) for photographic assistance, D. Mclean (Northwestern University) for his drawing skill, M. Farrar (Messiah College) for the mTdTomato construct and T. Porri (Cornell University) for performing the CT scans.

Author contributions

D.S., K.E.K., D.M.C, D.G.O., N.A., C.X. and J.R.F. contributed to experimental design and conceptual ideas. D.S and D.G.O. built and maintained the three-photon microscopes. K.E.K, D.M.C., D.S., D.G.O. and N.A. performed three-photon imaging experiments of zebrafish. Analysis was conducted by D.M.C., D.S., N.A. and K.E.K. R.T. and N.A. performed *Danionella* three-photon imaging. A.B. and J.R.F. supervised *Danionella* imaging and analysis. J.R.F. and D.M.C. prepared the manuscript with assistance from K.E.K. and input from all authors. J.R.F. and C.X. supervised all aspects of the project.

Competing interests

The authors declare no competing interests.

Additional information

Extended data is available for this paper at https://doi.org/10.1038/s41592-020-0819-7.

Supplementary information is available for this paper at https://doi.org/10.1038/s41592-020-0819-7.

Correspondence and requests for materials should be addressed to C.X. or J.R.F.

Peer review information Nina Vogt was the primary editor on this article and managed its editorial process and peer review in collaboration with the rest of the editorial team

Reprints and permissions information is available at www.nature.com/reprints.

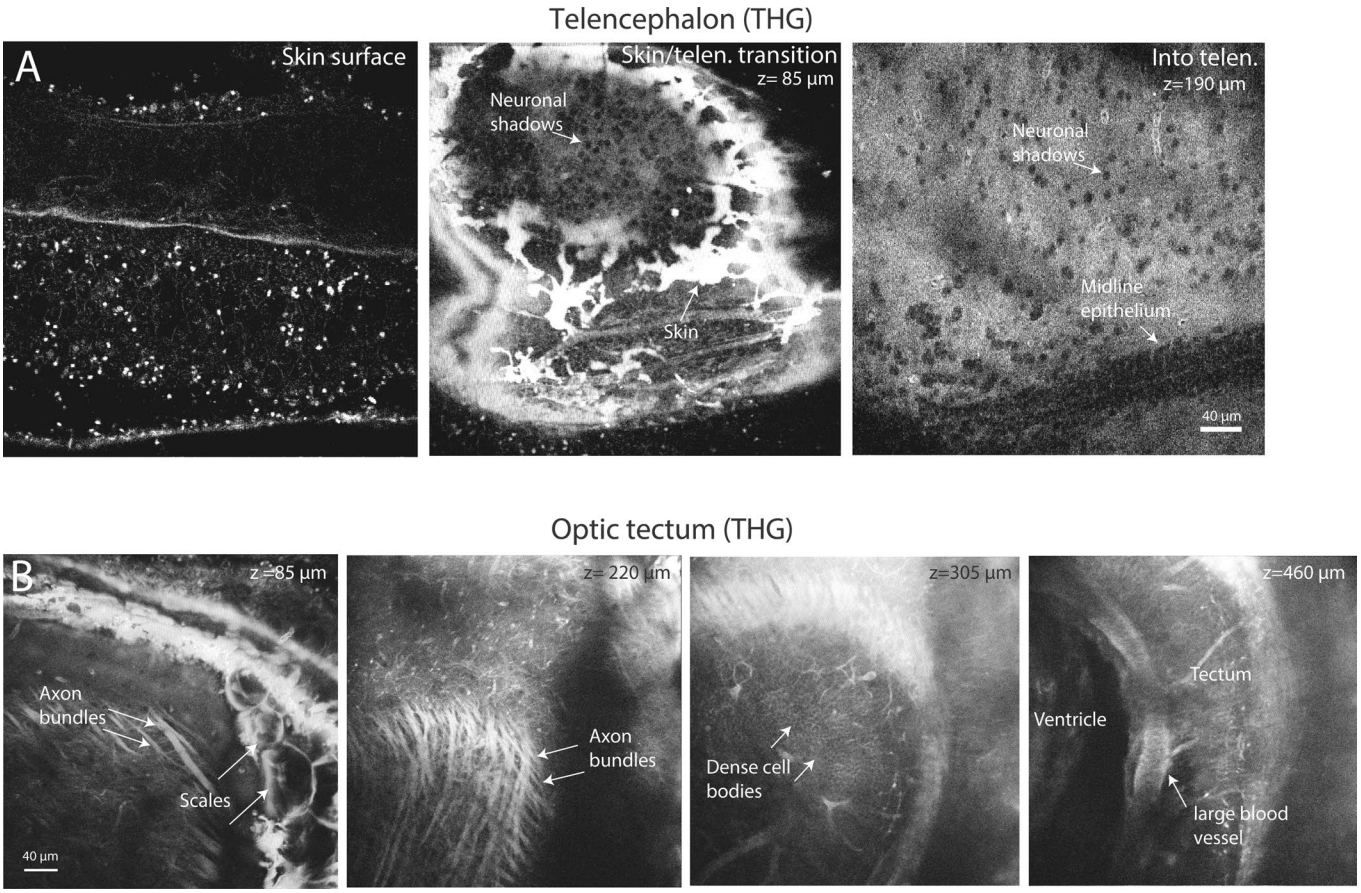

Extended Data Fig. 1 | Structural features visible in optical sections with THG that facilitate navigation through the brain. A. Telencephalic region, showing from left to right: the skin surface features; the transition into the brain as shadows of neurons become visible; and deeper in the telencephalon where the shadows of the neurons clustered at the midline are evident, as are scattered neurons throughout the section. **B**. Optic Tectum, showing from left to right: axon bundles on the surface of the tectum just below the skin and skull, with scales on the skin visible; deeper axon bundles in fiber layers of the tectum; densely packed shadows of cell bodies deep in the tectum; a major blood vessel lying adjacent to the ventricle deep in tectum. OT N= 16, Tel N=12.

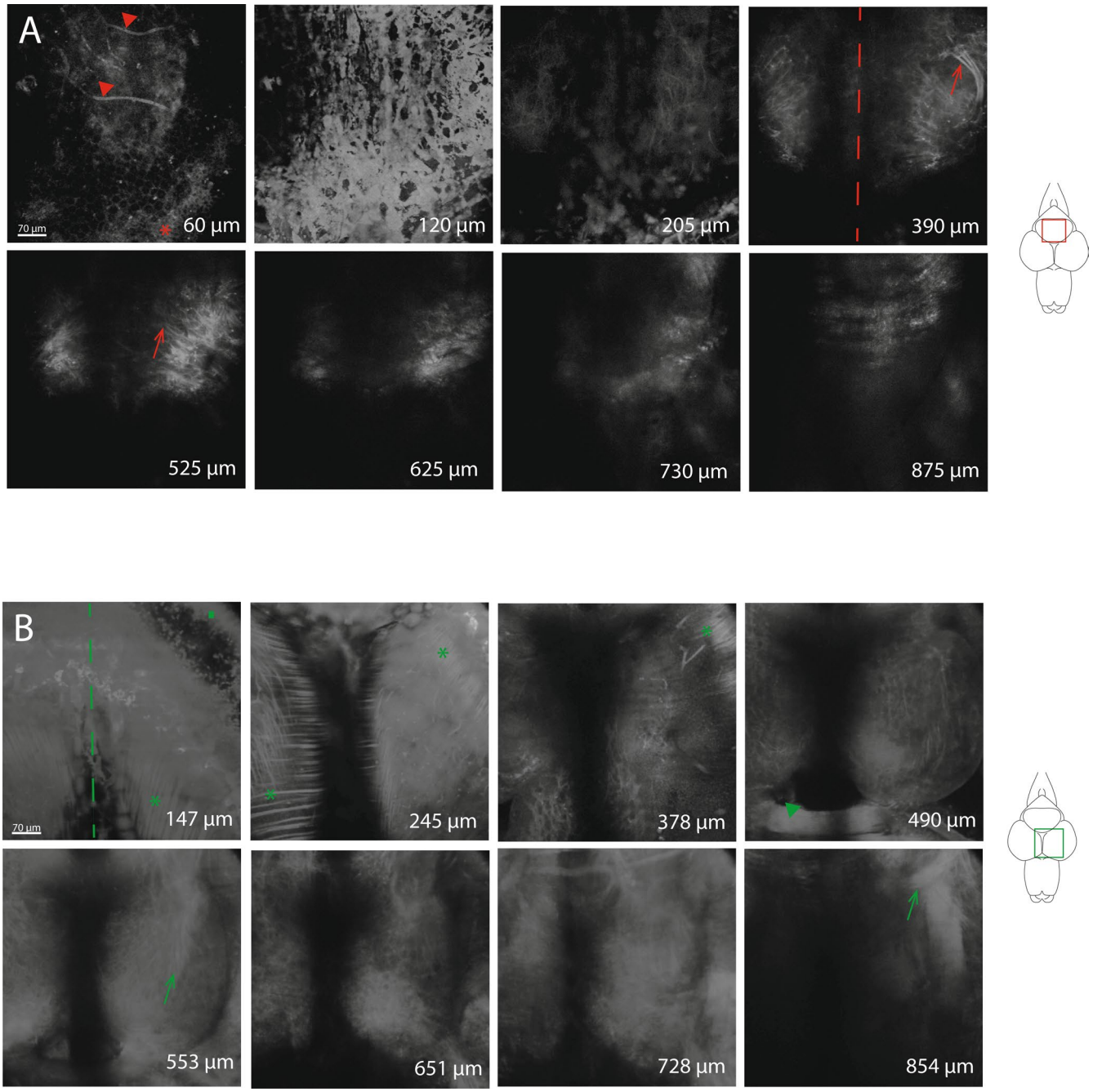

Extended Data Fig. 2 | Third harmonic generation images at different depths in the cerebellar and optic tectal areas. Squares on brain diagrams on the right show approximate areas of imaging, and dashed lines represent approximate brain midlines. **a**, Cerebellar region from shallow to deep imaging. At 60 µm, some skin is visible (red asterisk) due to the curvature of the brain, as well as several blood vessels (red triangles) under the skin and above the skull. At 120 µm, skull features are evident. Deeper into the brain, fiber tracts predominate (red arrows). **b**, Optic tectal region from shallow to deep. At 147 µm, some skull is evident (green square) as well as some brain. Tectal fiber tracts are evident (green asterisk) at multiple depths (see 147, 245 and 378 µm) with a thick commissural fiber tract present (green triangle) at 490 µm. At deeper layers fiber tracts predominate (green arrows). CB N=10, OT N=16.

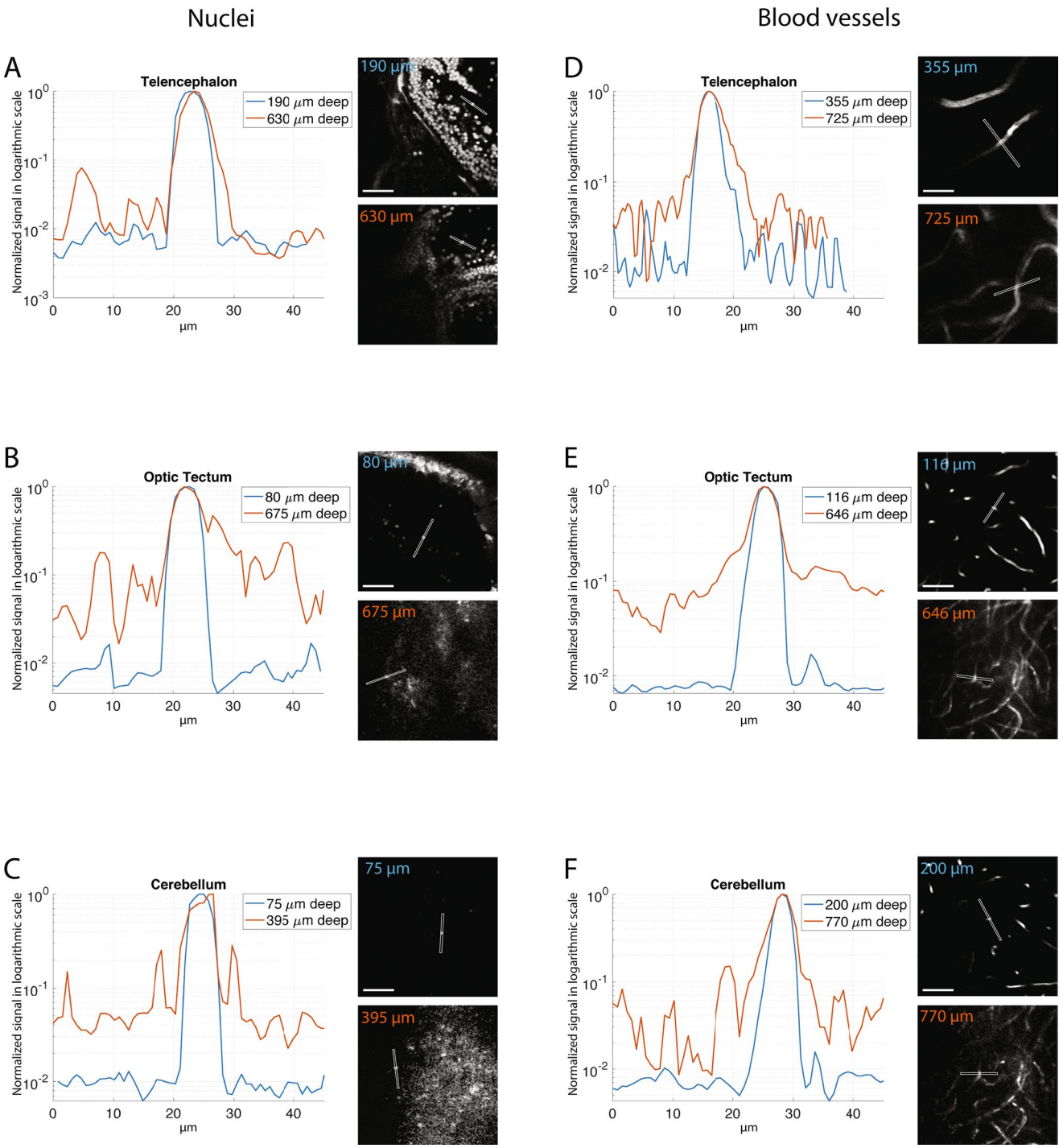

Extended Data Fig. 3 | Signal to Background ratio. Signal-to-background ratio (SBR) in shallow and deep regions in three areas of the brain. **a**–**c**, Fluorescence intensity profiles along the lines across GCaMP6s-labeled neuronal nuclei (N=1 each). **d**–**f**, Fluorescence intensity profiles along the lines across blood vessels labelled with fluorescein (N=2 each). To produce each plot, a five-pixel-wide line was drawn across the blood vessel or nucleus. The 5 pixel values were averaged to get an intensity value for the corresponding position along the line. The x axis corresponds to the lines shown on the images to the right. Scale bar 50 μm.

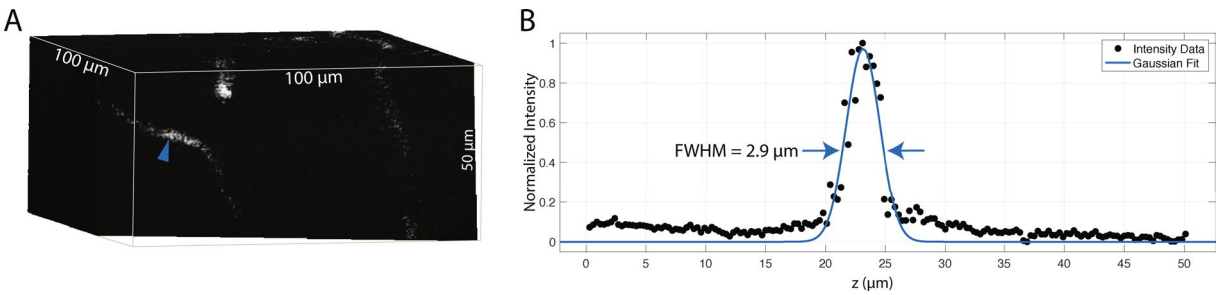

Extended Data Fig. 4 | 3P Axial resolution measurement. a, 3P image of a small fluorescein-labeled blood vessel (blue arrowhead) imaged about 200 µm deep into the optic tectum. Image stack was taken with 0.3 µm axial steps at 3 µs pixel time (512x512 pixels/frame) and 4 times averaging. **b**, Intensity profile along the axial direction fitted with a Gaussian curve to characterize the upper bound of axial resolution. The full width at half maximum of the Gaussian fit is 2.9 µm. N=1.

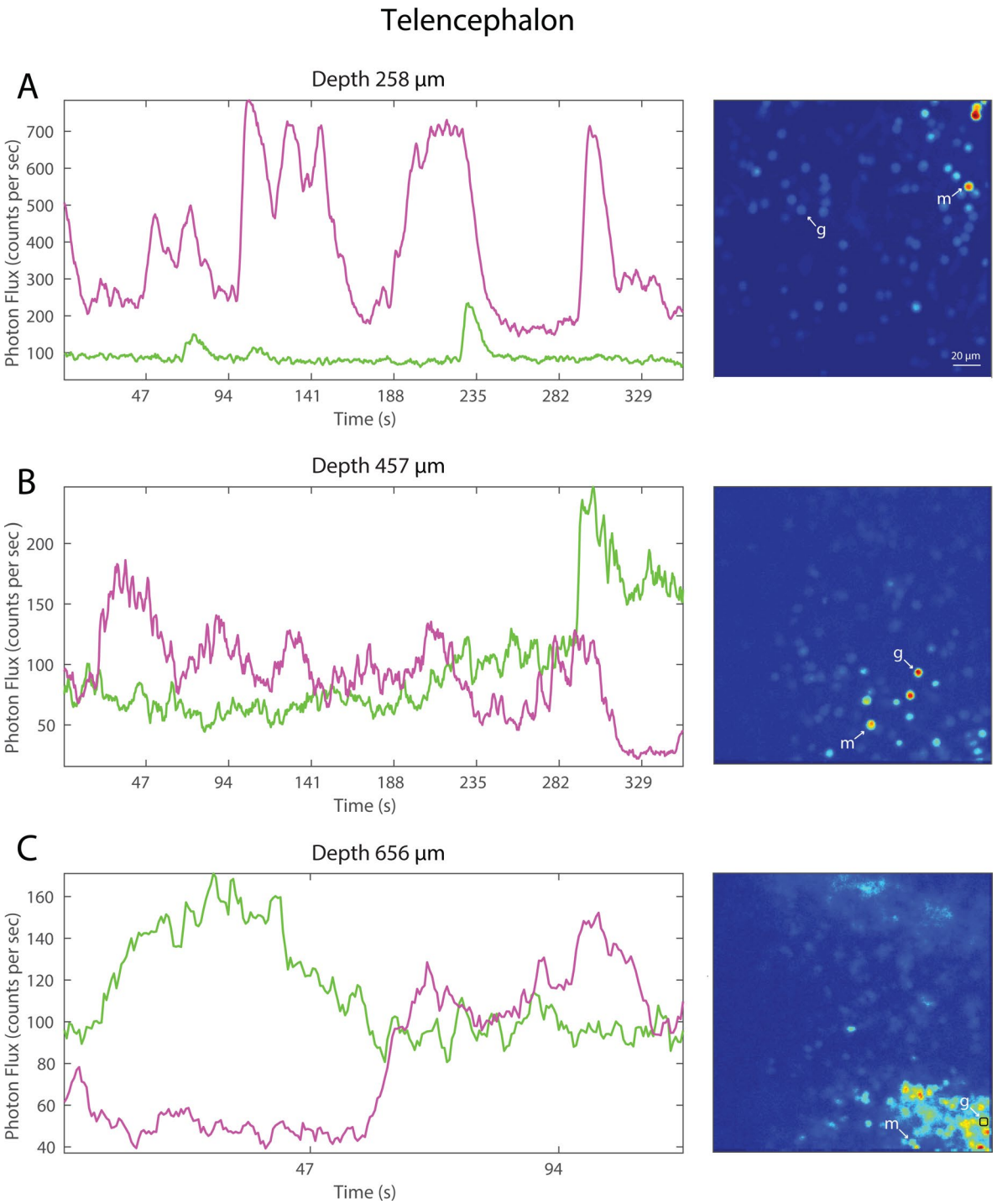

Extended Data Fig. 5 | Example photon counts from telencephalic neurons. Rows **a**–**c**, show neurons at different depths. In each panel, the plots in magenta and green show photon counts from two neurons at that depth, with the monitored neurons marked with m and g in the optical section shown at the right. Telencephalon functional imaging N= 9.

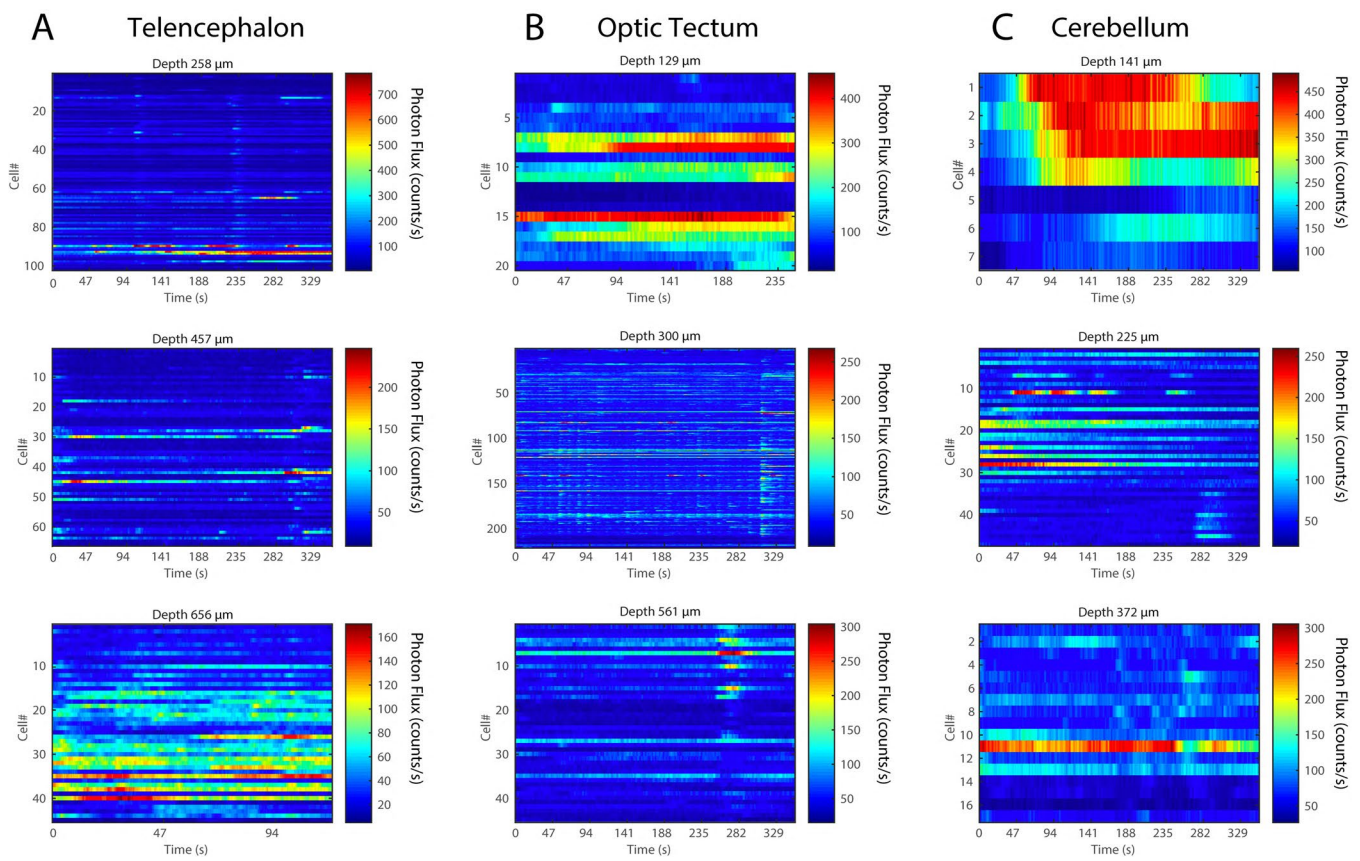

Extended Data Fig. 6 | Raster plot of photon counts for all of the neurons shown in main Fig. 2. Neurons were monitored at different depths in: **A**. telencephalon, **B**. optic tectum and **C**. cerebellum. Functional imaging: Tel N = 9, OT N = 6, CB N = 2.

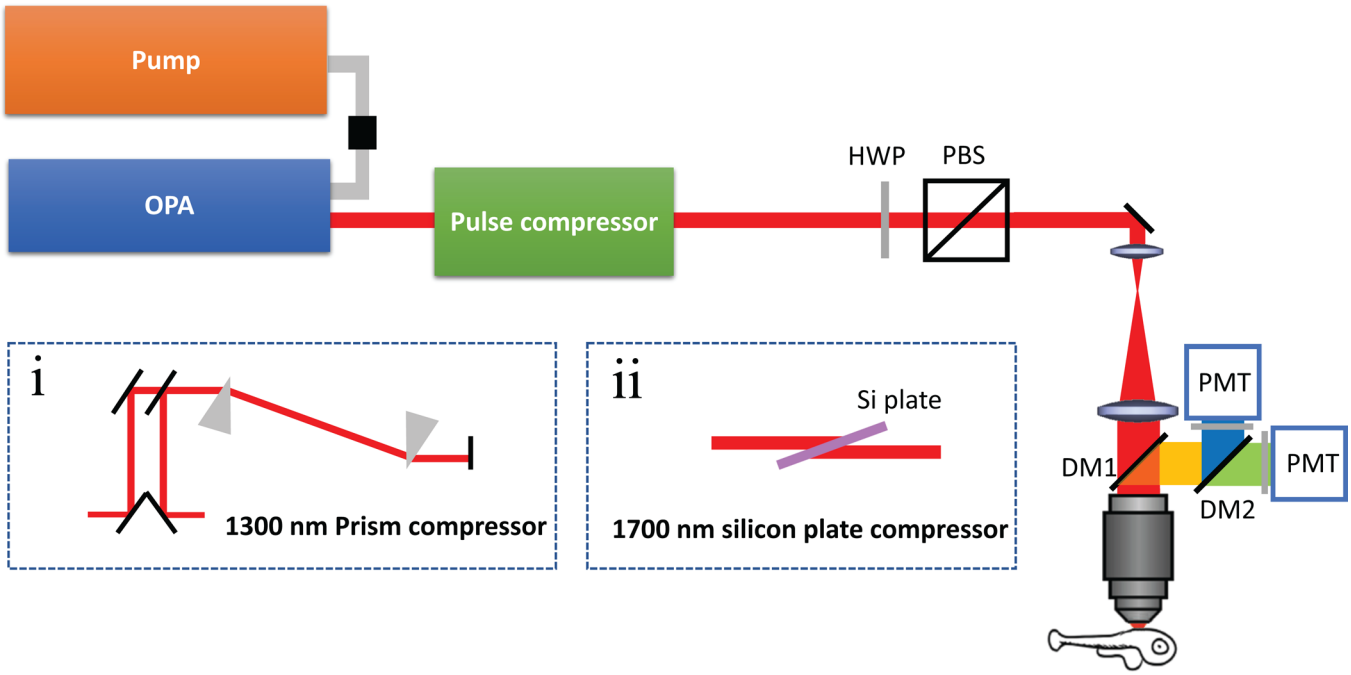

Extended Data Fig. 7 | Experimental setup. (**a**) schematic drawing of the excitation sources and the optical path of the imaging setup. OPA – optical parametric oscillator, HWP – Half wave plate, PBS – Polarizing Beam splitter, DM – Dichroic mirror, PMT – Photomultiplier tube. inset(i) - Optical path for the prism compressor for the 1300 nm setup. inset(ii) - Optical path for the silicon plate compressor for the 1700 nm setup.